

Subset method for one-dimensional QCD

Jacques Bloch, Falk Bruckmann, and Tilo Wettig

Institute for Theoretical Physics, University of Regensburg, 93040 Regensburg, Germany

E-mail: jacques.bloch@ur.de, falk.bruckmann@ur.de, tilo.wettig@ur.de

ABSTRACT: We present a subset method which solves the sign problem for QCD at nonzero quark chemical potential in 0+1 dimensions. The subsets gather gauge configurations based on the center symmetry of the $SU(3)$ group. We show that the sign problem is solved for one to five quark flavors and that it slowly reappears for a larger number of flavors. We formulate an extension of the center subsets that solves the sign problem for a larger number of flavors as well. We also derive some new analytical results for this toy model.

KEYWORDS: Lattice QCD, Quark chemical potential, Sign problem

Contents

1	Introduction	1
2	QCD in 0+1 dimensions	3
3	Subset method for $N_f = 1$	4
3.1	Subset construction and properties	4
3.2	Partition function and observables	6
3.3	Polyakov loop	7
3.4	Phase diagram	8
3.5	Simulation results	9
4	N_f larger than one	11
4.1	$N_f = 2$	12
4.2	Larger N_f	13
4.3	Extended subsets	17
5	Summary	21
A	One-flavor determinant	22
B	Some integrals of traces	23
C	Relation between quark number density and Polyakov loop	23
D	SU(3) eigenvalue representation	25
E	Average phase in the phase-quenched theory	25

1 Introduction

Numerical simulations of quantum chromodynamics (QCD) at nonzero quark chemical potential are seriously hampered by the sign problem, caused by the fluctuating sign of the fermion determinant. Although this sign problem is particularly serious in the four-dimensional theory, it is already apparent in (0+1)-dimensional QCD (QCD₁) [1]. Thus QCD₁ can be used as a toy model to study the sign problem [2], which is the main focus of the present paper. The sign problem in QCD₁ is actually mild such that reweighting methods can be used in simulations. Nevertheless, it is worthwhile to attempt to solve the sign problem exactly since such a solution could help us to better cope with the sign problem in higher-dimensional gauge theories.

A very general method that has been used in the past to solve or alleviate a number of sign problems can be called “subset method”. In this method, configurations appearing in the ensemble are grouped into subsets such that the sum of the weights associated with these configurations is real and positive. This positivity implies that Markov chains of relevant subsets can be generated using importance sampling methods in Monte Carlo simulations. For example, in the dimer algorithm [3, 4], which is a reformulation of strong-coupling QCD, dimer and baryon loops are gathered into subsets in order to alleviate the sign problem. Subsets in which the configurations are related by Z_2 or Z_3 rotations were introduced to solve the sign problem exactly in simulations of spin models using cluster algorithms [5, 6] and to alleviate the sign problem in QCD [7–10]. Recently, a subset method was proposed that solves the sign problem in simulations of a random two-matrix model of QCD [11, 12]. In this method, the configurations in a subset are related by orthogonal rotations, and it has since been shown that the subset positivity is closely related to a projection on the canonical determinant with zero quark number [13]. Since even in 0+1 dimensions QCD has a richer structure than just the canonical partition function with zero quark number, this particular subset method is not applicable to QCD.

In this work we investigate the idea to construct subsets with real and positive weights in the context of QCD, and specifically focus on QCD_1 . Our present application of the subset idea to an $\text{SU}(3)$ gauge theory is fundamentally different from the subset method applied to random matrix theory. Indeed, the rotations applied in the latter are not allowed in QCD as they would move the configurations outside the simulated theory. Instead, the subset construction proposed here is based on the Z_3 center symmetry of the $\text{SU}(3)$ group. As mentioned above, the idea of Z_3 averaging has been successfully applied in other theories before. In our case of QCD_1 , pure Z_3 rotations solve the sign problem, but only for a small number of flavors. We then introduce an extension of the subset construction that solves the sign problem also for a higher number of flavors.¹

Note that there is also a severe sign problem in the $\text{U}(3)$ theory in one dimension [2, 14, 15]. However, this sign problem can readily be solved as the subset method developed for random matrix theory can be directly ported to this gauge theory. We will not consider this theory further in this work as its physical content, i.e., the lack of baryons, is clearly different from that of QCD.

The structure of this paper is as follows. In section 2 we briefly review QCD_1 . In section 3 we present the subset construction based on pure Z_3 rotations for a single flavor and show analytically and through numerical simulations that it solves the sign problem. In section 4 we apply the subset method to a larger number of flavors and observe that the sign problem reappears for six or more flavors. We show how the remaining sign problem can be solved by an extension of the subset construction. A summary is given in section 5. We also compute a number of new analytical results, some of which are used to check the numerical simulations. Details on their derivation are provided in several appendices.

¹Note that for a single flavor the sign problem in QCD_1 could also be solved exactly using the dimer algorithm [3, 4], although this method was not yet explicitly applied to QCD_1 .

2 QCD in 0+1 dimensions

The system we analyze is an SU(3) gauge theory on a lattice with zero spatial extent and N_t sites in the temporal direction, whose physical extent is the inverse temperature $1/T = N_t a$, with a the lattice spacing. The one-dimensional Dirac operator for a quark of mass m at chemical potential μ reads [1]

$$aD = \begin{pmatrix} am & e^{a\mu}U_1/2 & 0 & \cdots & 0 & e^{-a\mu}U_{N_t}^\dagger/2 \\ -e^{-a\mu}U_1^\dagger/2 & am & e^{a\mu}U_2/2 & \cdots & 0 & 0 \\ \vdots & \vdots & \vdots & \ddots & \vdots & \vdots \\ 0 & 0 & 0 & \cdots & am & e^{a\mu}U_{N_t-1}/2 \\ -e^{a\mu}U_{N_t}/2 & 0 & 0 & \cdots & -e^{-a\mu}U_{N_t-1}^\dagger/2 & am \end{pmatrix}, \quad (2.1)$$

where U_1, \dots, U_{N_t} are the gauge links, and the opposite sign in front of U_{N_t} and $U_{N_t}^\dagger$ accounts for the antiperiodic boundary conditions of the fermions in the temporal direction. In the following we assume that N_t is even.

Via a gauge transformation all links in the temporal direction can be shifted into a single link, $U_1 \cdots U_{N_t} \equiv P$, where P is the Polyakov loop. Due to the low dimensionality, there is no field strength (i.e., no plaquette) and thus no gauge action. The partition function

$$Z^{(N_f)} = \int dP \det^{N_f}[aD(P)], \quad (2.2)$$

where dP is the Haar measure of SU(3), is thus simply a one-link integral of the determinant of the Dirac operator for N_f quark flavors, which for simplicity we take to be degenerate, coupled to a chemical potential μ . Expectation values of observables are defined in the usual way,

$$\langle O \rangle = \frac{1}{Z^{(N_f)}} \int dP \det^{N_f}[aD(P)] O(P). \quad (2.3)$$

One can show that (for even N_t) the Dirac determinant can be reduced to the determinant of a 3×3 matrix [1],

$$\det(aD) = \frac{1}{2^{3N_t}} \det(A \mathbb{1}_3 + e^{\mu/T} P + e^{-\mu/T} P^\dagger) \quad (2.4)$$

with

$$A = 2 \cosh(\mu_c/T) \quad (2.5)$$

and critical chemical potential [1, 2]

$$a\mu_c = \operatorname{arsinh}(am). \quad (2.6)$$

The chiral limit $m = 0$ correspond to $A = 2$. In the continuum limit $a \rightarrow 0$ one has $\mu_c \rightarrow m$. Equation (2.4) shows that $\det(aD)$ depends on P and μ only through the

combination $e^{\mu/T}P$. This is due to the facts that (i) all gauge links can be shifted into one, which then equals P , and (ii) the Dirac determinant depends on μ only through closed temporal loops, which give rise to a factor of $(e^{a\mu})^{N_t} = e^{\mu/T}$. From now on we set $a = 1$.

The determinant (2.4) can be decomposed into powers of $e^{\mu/T}$ as

$$\det D(P) = \sum_{q=-3}^3 D_q(P) e^{q\mu/T}, \quad (2.7)$$

where the coefficients D_q are the canonical determinants.² From now on we omit the irrelevant prefactor $1/2^{3N_t}$ in (2.4) such that the first and the last term on the RHS of (2.7) have unit coefficients, i.e., $D_{-3} = D_3 = 1$. The coefficients D_q are given in appendix A. They depend on the configuration, i.e., the Polyakov loop, and are generically complex. From eq. (2.4) we see that $\det D(\mu) = \det D^\dagger(-\mu)$ such that the canonical determinants satisfy $D_q^* = D_{-q}$. The imaginary parts of the coefficients D_q can be cancelled by pairing each Polyakov loop with its complex conjugate (in the same spirit as in the subsets below), as $\det D(P^*) = [\det D(P)]^*$.³ The sum of the determinants for P and P^* is real, but without a definite sign. The fact that these real parts can have fluctuating signs causes the sign problem in probability-based approaches to the path integral. At vanishing μ the Dirac operator has complex conjugate pairs of eigenvalues such that its determinant is real and nonnegative.

3 Subset method for $N_f = 1$

3.1 Subset construction and properties

We first demonstrate the subset method for the one-flavor partition function. The aim of the subset method is to gather configurations of the ensemble into small subsets such that the sum of their weights contributing to the partition function is real and nonnegative. This basic idea is identical to that proposed for random matrix theory in refs. [11, 12], but the generation of the subsets will be fundamentally different, mainly because of the stringent constraint that the configurations be elements of the $SU(3)$ gauge group.

In the proposed subset method, starting from a seed configuration P a subset Ω_P is formed containing three $SU(3)$ elements:⁴ the seed configuration itself and the $SU(3)$ elements generated by rotating the seed by the two nontrivial center elements of $SU(3)$,

$$\Omega_P = \{P, e^{2\pi i/3}P, e^{4\pi i/3}P\}. \quad (3.1)$$

For any $P \in SU(3)$, the rotated configurations are again elements of $SU(3)$ and thus part of the ensemble. As the subsets are invariant under Z_3 rotations, the set of all subsets

²For general gauge group $SU(N_c)$ the lowest and highest powers are $\pm N_c\mu/T$.

³In QCD_1 we could alternatively pair P with P^\dagger instead of P^* since $\det D(P^\dagger) = [\det D(P)]^*$ in this case, see (2.4). However, in higher dimensions $\det(\{U^\dagger\}) \neq [\det D(\{U\})]^*$, while $\det D(\{U^*\}) = [\det D(\{U\})]^*$ always holds.

⁴For gauge group $SU(N_c)$ the subset method is generalized in a straightforward way with N_c configurations in each subset.

forms a three-fold covering of the original SU(3) ensemble. Therefore, we define the subset weights as

$$\sigma(\Omega_P) = \frac{1}{3} \sum_{k=0}^2 \det D(P_k) \quad (3.2)$$

with $P_k = e^{2\pi ik/3} P$. Note that any of the three configurations can be used as a seed of the subset. As the Haar measure dP is invariant under the center rotations, the QCD₁ partition function can be rewritten as an integral over the subsets,

$$Z^{(1)} = \int dP \sigma(\Omega_P). \quad (3.3)$$

To compute observables one has to take into account that the three configurations in a subset can have different values of the observable, such that

$$\langle O \rangle = \frac{1}{Z^{(1)}} \int dP \sigma(\Omega_P) \langle O \rangle_{\Omega_P} \quad (3.4)$$

with subset measurements

$$\langle O \rangle_{\Omega_P} = \frac{1}{3\sigma(\Omega_P)} \sum_{k=0}^2 \det D(P_k) O(P_k), \quad (3.5)$$

where $P_k \in \Omega_P$ and $\langle 1 \rangle_{\Omega} = 1$. The measure $dP \sigma(\Omega_P)$ in eq. (3.4) indicates that subsets of configurations, rather than individual configurations, will be generated in the numerical simulations, such that observables will be approximated as sample means of N_{MC} subset measurements,

$$\bar{O} = \frac{1}{N_{\text{MC}}} \sum_{n=1}^{N_{\text{MC}}} \langle O \rangle_{\Omega_n}. \quad (3.6)$$

The subset weights σ are the main ingredients of the method, and their properties will now be analyzed further. From eq. (2.4) we observe that multiplying the Polyakov loop by a phase factor $e^{i\theta}$ can be reinterpreted as adding an imaginary part $i\theta$ to the chemical potential μ/T [13],

$$\det D(e^{i\theta} P) \Big|_{\mu/T} = \det D(P) \Big|_{\mu/T+i\theta}. \quad (3.7)$$

While this relation holds for any angle θ , we will only use $\theta = 0, 2\pi/3, 4\pi/3$ for the rotations of P in order to remain in the gauge group. By applying eq. (3.7) to the subset weight (3.2) we find that the sum of determinants in a subset effectively projects the determinant (2.7) onto its components with zero triality ($q \bmod 3 = 0$),⁵

$$\sigma(\Omega_P) = \frac{1}{3} \sum_{k=0}^2 \sum_{q=-3}^3 D_q(P) e^{q(\mu/T+2\pi ik/3)} = \sum_{b=-1}^1 D_{3b}(P) e^{3b\mu/T}, \quad (3.8)$$

⁵Here we see the difference to the random-matrix model [11–13] and gauge theories with gauge group U(N), see, e.g., [16]. In those cases, the configuration space allows for rotations by arbitrary angles θ such that the subsets project onto the sector with vanishing quark number. As a result, the partition function does not depend on μ at all.

where in the last step we changed the summation index from q (“quark number”) to b (“baryon number”). The last equality follows from the well-known formula for the sum of the q -th powers of the N -th roots of unity, $\sum_{k=0}^{N-1} \exp(2\pi i q k / N) = N \delta_{q \bmod N, 0}$. As the same expansion (3.8) can be derived using any of the three subset elements as the seed for the subset, it follows that the canonical determinants with triality zero are identical for the three subset elements. In section 4 we will show that this projection cures, or at least attenuates, the sign problem depending on the number of flavors being considered.

As the partition function can be written as an integral over the subsets, we obtain from (3.8) the fugacity expansion

$$Z^{(1)}(\mu) = \sum_{b=-1}^1 Z_{3b}^{(1)} e^{3b\mu/T} \quad (3.9)$$

with canonical partition functions

$$Z_q^{(1)} = \int dP D_q(P). \quad (3.10)$$

The absence of the other triality contributions ($q \bmod 3 \neq 0$) is a direct consequence of the center symmetry of $SU(3)$. Although the determinants of the individual configurations contribute to all triality sectors, the subset approach, by making use of the center symmetry, automatically projects onto the only triality sector that contributes to the overall partition function.

Let us rewrite eq. (3.8) as

$$\sigma(\Omega_P) = D_0(P) + 2 \cosh(3\mu/T). \quad (3.11)$$

The second term is obviously positive, and from (A.7) the constant term is

$$D_0(P) = A^3 + A(|\operatorname{tr} P|^2 - 3) \quad (3.12)$$

with $A = 2 \cosh(\mu_c/T) \geq 2$ and $|\operatorname{tr} P| \in [0, 3]$ such that D_0 is positive, too. Therefore, the subset weight $\sigma(\Omega_P)$ is real and positive for any m , μ , and P and can be used to generate subsets with importance sampling in Markov chain Monte Carlo methods.

3.2 Partition function and observables

Once we have formulated the partition function in terms of subsets, it can be computed analytically by performing a group integration of eq. (3.11), which yields

$$Z^{(1)} = A^3 - 2A + 2 \cosh(3\mu/T), \quad (3.13)$$

where we used $\int dP |\operatorname{tr} P|^2 = 1$ as shown in appendix B. Using the definition of A this can be rewritten as

$$Z^{(1)} = \frac{\sinh(4\mu_c/T)}{\sinh(\mu_c/T)} + 2 \cosh(3\mu/T), \quad (3.14)$$

which agrees with the literature [1, 2]. From the partition function (3.13) we can easily compute the chiral condensate as its mass derivative,

$$\Sigma = T \frac{\partial \log Z^{(1)}}{\partial m} = \frac{1}{Z^{(1)}} \frac{4 \sinh(\mu_c/T)}{\cosh(a\mu_c)} [5 + 6 \sinh^2(\mu_c/T)], \quad (3.15)$$

where we have used (2.6) and temporarily restored the lattice spacing a . Note that the discretization-dependent factor $\cosh(a\mu_c)$ goes to one in the continuum limit. From (3.15) we see that the μ -dependence of the chiral condensate is given by the inverse partition function, so asymptotically it behaves like $e^{-3|\mu|/T}$.

The quark number density is computed by taking the derivative of the partition function with respect to the chemical potential,

$$n = T \frac{\partial \log Z^{(1)}}{\partial \mu} = \frac{6 \sinh(3\mu/T)}{Z^{(1)}}. \quad (3.16)$$

For large μ we find the expected saturation

$$\lim_{\mu \rightarrow \pm\infty} n = \frac{6 \sinh(3\mu/T)}{2 \cosh(3\mu/T)} \rightarrow \pm 3. \quad (3.17)$$

3.3 Polyakov loop

Another observable of interest, which, however, cannot be computed directly as a derivative of the partition function, is the trace of the Polyakov loop. Below, we show that its expectation value,

$$\langle \text{tr } P \rangle = \frac{1}{Z^{(1)}} \int dP \det D(P) \text{tr } P = \frac{1}{Z^{(1)}} \int dP \sigma(\Omega_P) \langle \text{tr } P \rangle_{\Omega_P} \quad (3.18)$$

can elegantly be computed using the subset construction. To do so, one needs to evaluate the subset measurement (3.5),

$$\langle \text{tr } P \rangle_{\Omega_P} = \frac{1}{3\sigma} \sum_{k=0}^2 \det D(P_k) \text{tr } P_k. \quad (3.19)$$

Under the center rotations the Polyakov loop traces transform as $\text{tr } P_k = e^{2\pi ik/3} \text{tr } P$, and we compute along the lines of (3.8)

$$\begin{aligned} \langle \text{tr } P \rangle_{\Omega_P} &= \frac{1}{3\sigma} \sum_{k=0}^2 \sum_{q=-3}^3 D_q(P) e^{q(\mu/T + 2\pi ik/3)} \times e^{2\pi ik/3} \text{tr } P \\ &= \frac{1}{\sigma} \left[D_{-1}(P) e^{-\mu/T} + D_2(P) e^{2\mu/T} \right] \text{tr } P. \end{aligned} \quad (3.20)$$

In contrast to the case of the subset weights, a different triality sector ($q \bmod 3 = -1$) contributes to the subset measurement of the Polyakov loop. Substituting eqs. (A.8) and (A.9) into eq. (3.4) and integrating over P using appendix B we obtain

$$\langle \text{tr } P \rangle = \frac{(A^2 - 1) e^{-\mu/T} + A e^{2\mu/T}}{A^3 - 2A + 2 \cosh(3\mu/T)}. \quad (3.21)$$

Similarly, the expectation value of the anti-Polyakov loop P^\dagger will only contain terms with $q \bmod 3 = 1$, and we have

$$\langle \text{tr } P^\dagger \rangle = \frac{A e^{-2\mu/T} + (A^2 - 1) e^{\mu/T}}{A^3 - 2A + 2 \cosh(3\mu/T)} = \langle \text{tr } P \rangle \Big|_{\mu \rightarrow -\mu}. \quad (3.22)$$

For very large chemical potential, the Polyakov loop decays exponentially as it is suppressed by the partition function in the denominator,

$$\langle \text{tr } P \rangle \sim \begin{cases} e^{2\mu/T}, & \mu \rightarrow -\infty, \\ e^{-\mu/T}, & \mu \rightarrow \infty, \end{cases} \quad \langle \text{tr } P^\dagger \rangle \sim \begin{cases} e^{\mu/T}, & \mu \rightarrow -\infty, \\ e^{-2\mu/T}, & \mu \rightarrow \infty. \end{cases} \quad (3.23)$$

Note that $\langle \text{tr } P^\dagger \rangle \neq \langle \text{tr } P \rangle$ since the weight with which the average is performed is complex, i.e., the real part of the expectation value of $\text{tr } P$ is obtained by integrating over $\text{Re}(\det D) \text{Re}(\text{tr } P) - \text{Im}(\det D) \text{Im}(\text{tr } P)$. For $\text{tr } P^\dagger$ the sign of the second term will be reversed, such that different contributions will arise. Note further that the average Polyakov loop is real. This is because P^* , which is also part of the $\text{SU}(3)$ ensemble, gives a contribution of $(\det D \text{tr } P)^*$ that cancels the imaginary part in the average.

Since a positive quark chemical potential favors quarks over antiquarks, their free energies should differ at nonzero chemical potential. This is achieved by the aforementioned asymmetry between the expectation values of $\text{tr } P$ and $\text{tr } P^\dagger$ [17]. If we invert the sign of the chemical potential the roles of quarks and antiquarks are merely interchanged, and we obtain $\langle \text{tr } P^\dagger \rangle_\mu = \langle \text{tr } P \rangle_{-\mu}$.

The quantities $e^{\mu/T} \langle \text{tr } P \rangle$ and $e^{-\mu/T} \langle \text{tr } P^\dagger \rangle$ only contain triality zero sectors, and from (3.16) we see that their difference is related to the quark number as

$$n = \frac{3}{A} \langle e^{\mu/T} \text{tr } P - e^{-\mu/T} \text{tr } P^\dagger \rangle. \quad (3.24)$$

In appendix C we derive relations between the quark number density and the Polyakov loop for an arbitrary number of flavors.

3.4 Phase diagram

We briefly discuss the phase diagram of QCD_1 for one flavor, which can be derived using the analytical formulas for chiral condensate, number density, and Polyakov loop.

In figure 1 we show the quark number density, the chiral condensate, and the trace of the Polyakov and anti-Polyakov loop versus chemical potential and temperature for $m = 0.3$. A true phase transition only occurs at $T = 0$ and $\mu = \mu_c$, where the partition function (for $\mu > 0$) is given by

$$\lim_{T \rightarrow 0} Z^{(1)} = \lim_{T \rightarrow 0} (e^{3\mu/T} + e^{3\mu_c/T}). \quad (3.25)$$

From this expression we see that for $T \rightarrow 0$ and $\mu < \mu_c$ the partition function and all thermodynamic observables are independent of μ (a fact that has been termed the Silver Blaze property [18]), while for $T \rightarrow 0$ and $\mu > \mu_c$ the partition function and all thermodynamic

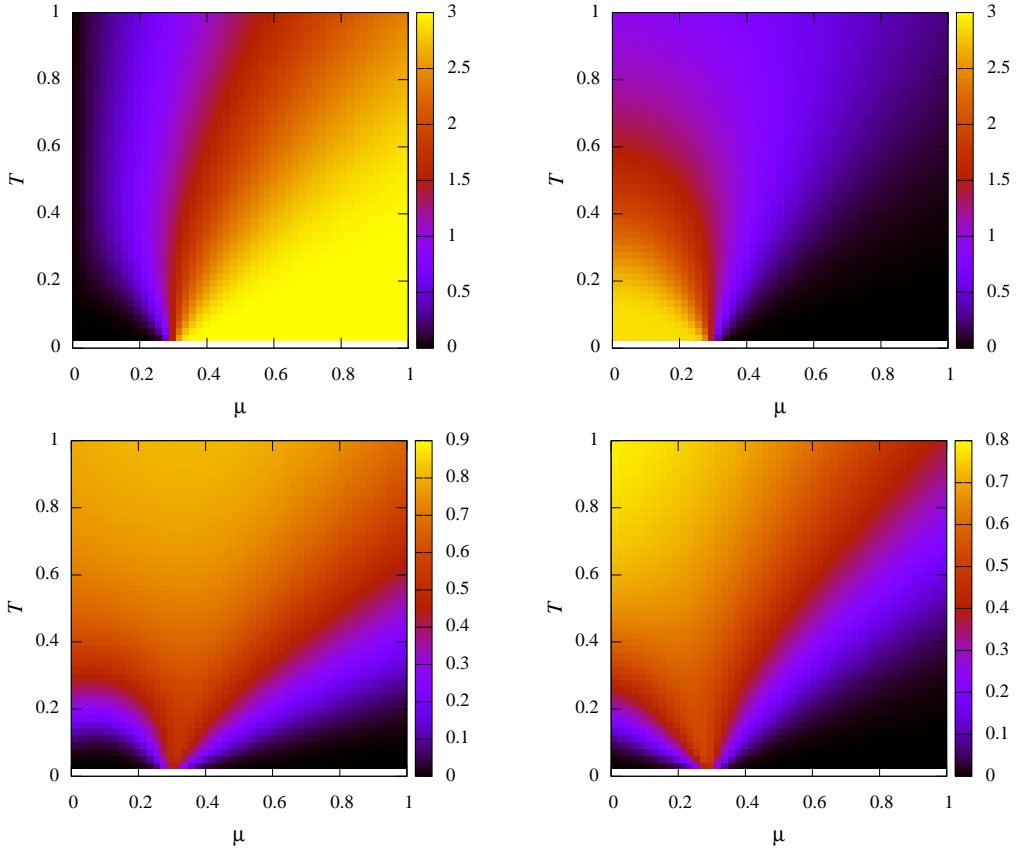


Figure 1. (μ, T) -diagram for the number density (top left), chiral condensate (top right), Polyakov loop (bottom left), and anti-Polyakov loop (bottom right) for $m = 0.3$.

observables are independent of m (which can be viewed as an analog of the Silver Blaze property).

Note that the partition function does not depend separately on the three variables m , μ , and T but only on the two ratios μ/T and μ_c/T , where μ_c is related to m via (2.6). Therefore it is interesting to look at the observables as a function of these two scaled variables, see figure 2. Here we defined the modified chiral condensate $T\partial\log Z^{(1)}/\partial\mu_c = \Sigma \cosh(a\mu_c) = \Sigma \cosh(\frac{1}{N_t}\mu_c/T)$ to eliminate an explicit dependence on N_t .

3.5 Simulation results

Although most observables in QCD_1 can be computed by taking derivatives of the partition function or performing the integrals over the gauge group explicitly, the main aim of this work is to construct a numerical method that makes it possible to perform Monte Carlo simulations of this theory. We therefore implemented the subset method to verify that it reliably reproduces the analytical predictions. As the subset weights are real and positive we can generate Markov chains of relevant subsets using the Metropolis algorithm, where the full $\text{SU}(3)$ links were generated according to the Haar measure using the Bronzan algorithm [19]. We typically generated Markov chains with 100,000 subsets. As most

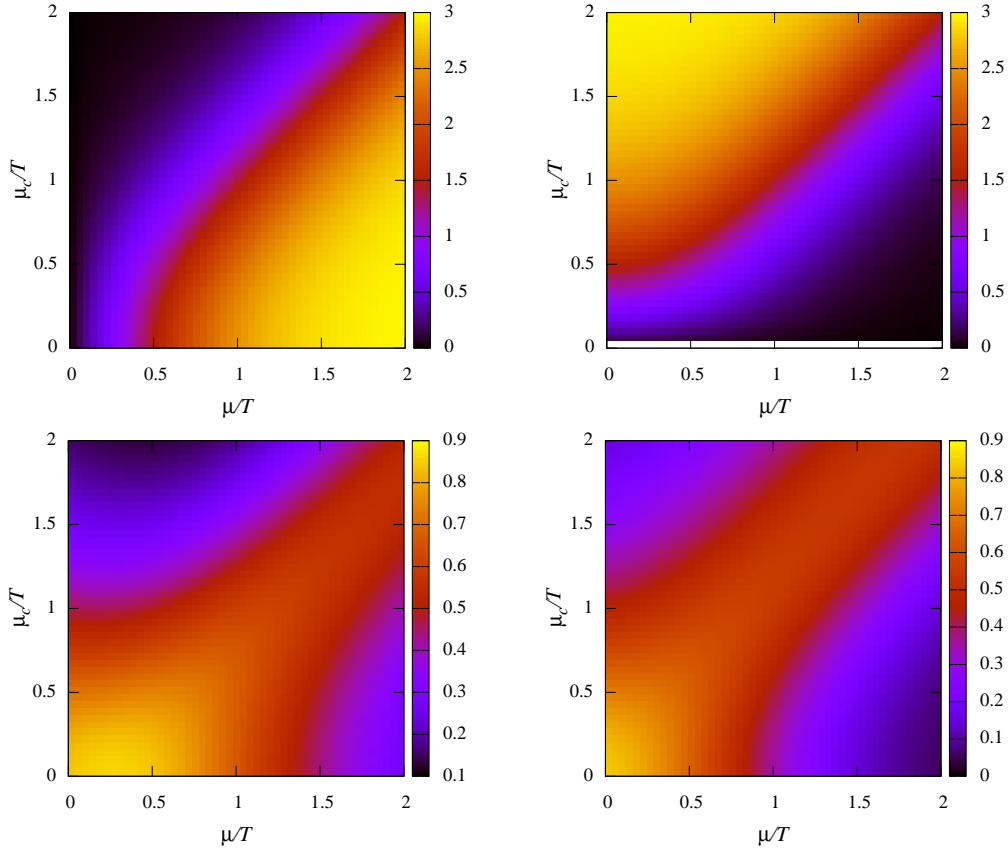


Figure 2. $(\mu/T, \mu_c/T)$ -diagram for the number density (top left), modified chiral condensate $T \partial \log Z^{(1)} / \partial \mu_c = \Sigma \cosh(a \mu_c)$ (top right), Polyakov loop (bottom left), and anti-Polyakov loop (bottom right).

results only depend on μ/T and μ_c/T (except for a prefactor in the chiral condensate), the simulations were performed using the minimally allowed time extent $N_t = 2$.⁶

By taking the mass and chemical potential derivatives of the partition function (2.2) we observe that the chiral condensate and quark number density can be computed as ensemble expectation values of the observables

$$O_\Sigma = \frac{1}{N_t} \text{tr} \left[D^{-1} \frac{\partial D}{\partial m} \right] = \frac{1}{N_t} \text{tr} [D^{-1}], \quad O_n = \frac{1}{N_t} \text{tr} \left[D^{-1} \frac{\partial D}{\partial \mu} \right]. \quad (3.26)$$

To compute the expectation values with the subset method we apply formula (3.6) with subset measurements (3.5).

We numerically computed the chiral condensate for different values of m using the subset method and found very good agreement with the analytical prediction of eq. (3.15) over several orders of magnitude, as can be seen in figure 3.

We also used our Monte Carlo simulations to compute the quark number density and compared the results with the analytical prediction (3.16) for the massless and massive cases in figure 4. As can be shown from the theoretical formula, the linear rise at $\mu = 0$ for

⁶We also performed simulations with $N_t > 2$ to verify the numerical results.

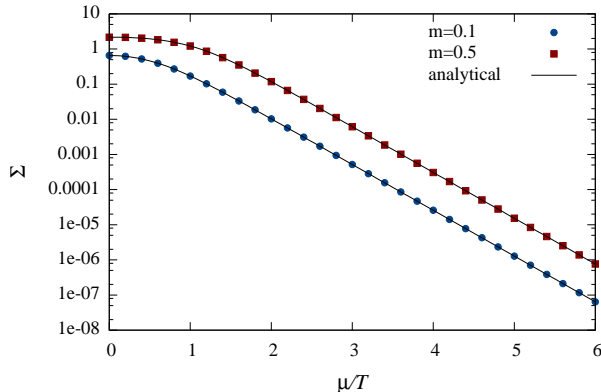


Figure 3. Chiral condensate as a function of μ/T for $N_t = 2$ and $N_f = 1$ with $m = 0.1$ and 0.5 . The solid lines are the analytical result (3.15) from [1]. The error bars are smaller than the symbols.

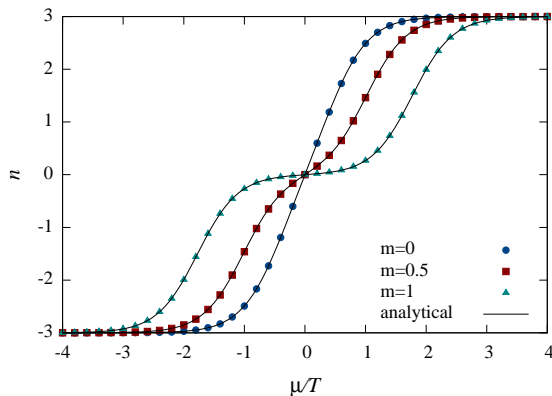


Figure 4. Quark number density as a function of μ/T for $N_f = 1$ with $m = (0, 0.5, 1)$. The solid lines represent the analytical result (3.16).

$m = 0$ is given by $n \sim 3\mu/T$. In the massive case, the number density still varies linearly with μ around $\mu = 0$, but the rise is much slower due to the large denominator in (3.16).

Finally, we measured the average trace of the Polyakov loop and compared the results with the prediction of eq. (3.21) in figure 5. We indeed observe the $\mu \leftrightarrow -\mu$ asymmetry (equivalent to the $\text{tr } P \leftrightarrow \text{tr } P^\dagger$ asymmetry) mentioned in section 3.3. This is clearly illustrated in the figure by the different exponential decays for large positive and negative μ as described by eq. (3.23). Measurements of the anti-Polyakov loop would merely correspond to a $\mu \rightarrow -\mu$ exchange.

4 N_f larger than one

We now analyze the subset method for larger N_f . As we will see below, the Z_3 subset method, introduced in section 3.1 for $N_f = 1$, completely removes the sign problem for $N_f \leq 5$. The sign problem then reappears for $N_f \geq 6$, and we discuss how it can be solved in this case. We start the discussion with $N_f = 2$.

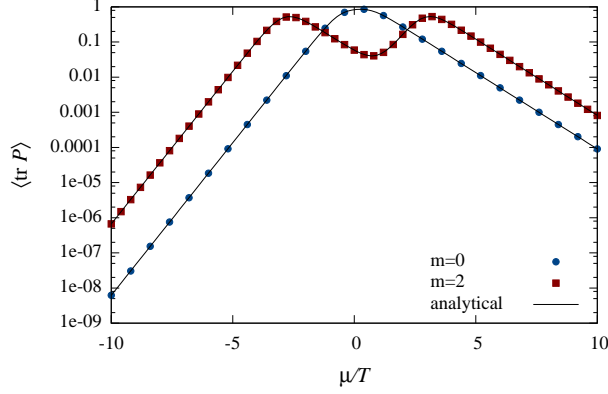


Figure 5. Average trace of the Polyakov loop $\langle \text{tr } P \rangle$ as a function of μ/T for $N_f = 1$ with $m = 0$ and $m = 2$. The solid lines correspond to the analytical formula (3.21).

4.1 $N_f = 2$

For two flavors the fermionic weight $\det^2 D$ can be decomposed (up to an irrelevant normalization factor) into

$$\det^2 D(P) = \sum_{q=-6}^6 D_q^{(N_f=2)} e^{q\mu/T}, \quad (4.1)$$

where the first and the last coefficient $D_{\pm 6}^{(N_f=2)}$ are unity again. The Z_3 subsets are defined in a similar way as for $N_f = 1$,

$$\Omega_P = \{P, e^{2\pi i/3} P, e^{4\pi i/3} P, P^*, e^{2\pi i/3} P^*, e^{4\pi i/3} P^*\}, \quad (4.2)$$

where we now also included the complex conjugate links P_k^* in Ω_P . Their determinants satisfy $\det D(P_k^*) = [\det D(P_k)]^*$, and thus the subset weight

$$\sigma_{N_f=2}(\Omega_P) = \frac{1}{6} \sum_{k=0}^2 \det^2 D(P_k) + \text{c.c.} \quad (4.3)$$

is guaranteed to be real.⁷ As before, only triality zero contributions survive in this sum,

$$\sigma_{N_f=2}(\Omega_P) = D_0^{(N_f=2)} + 2 \text{Re } D_3^{(N_f=2)} \cosh(3\mu/T) + 2 \cosh(6\mu/T). \quad (4.4)$$

The canonical determinants are computed by squaring eq. (A.6) and substituting (A.7)–(A.10),

$$\begin{aligned} D_0^{(N_f=2)} &= D_0^2 + 2(1 + |D_1|^2 + |D_2|^2) \\ &= (A^6 - 6A^4 + 9A^2 + 2) + 4(A^4 - 3A^2 + 2)|\text{tr } P|^2 + (A^2 + 2)|\text{tr } P|^4 \\ &\quad + 2(A^2 - 2)[(\text{tr } P)^3 + (\text{tr } P^\dagger)^3], \end{aligned} \quad (4.5)$$

$$D_3^{(N_f=2)} = 2(D_0 + D_1 D_2) = 2A[(A^2 - 3) + (A^2 - 1)|\text{tr } P|^2 + (\text{tr } P^\dagger)^3]. \quad (4.6)$$

⁷For $N_f = 1$ (and $N_f = 1$ only) the inclusion of the complex conjugate links P_k^* was not necessary since in this case the subset weight was real (and positive) to start with. See also footnote 3 for the reason why we added P_k^* and not P_k^\dagger .

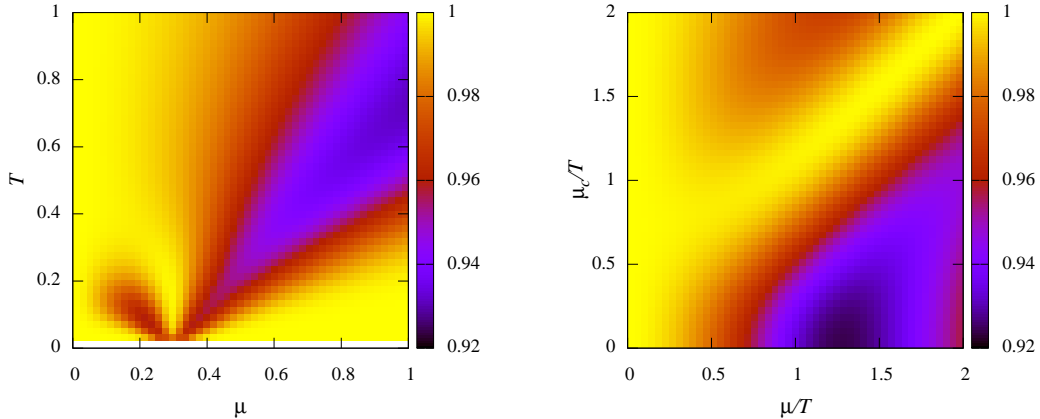


Figure 6. Average phase of the fermion determinant in the phase-quenched ensemble for $N_f = 2$, eq. (4.8), as a function of chemical potential and temperature for $m = 0.3$ (left) and as a function of the scaled variables μ/T and μ_c/T (right).

An analysis of these expressions shows that the subset weight $\sigma_{N_f=2}$ is positive for all Polyakov loops and all values of chemical potential and mass, such that it can be used to generate $N_f = 2$ subsets with importance sampling.

Once we know the subset weight, the partition function readily follows by integrating over the gauge configuration,

$$Z^{(2)} = (A^6 - 2A^4 + 3A^2 + 6) + 4A(2A^2 - 3) \cosh(3\mu/T) + 2 \cosh(6\mu/T), \quad (4.7)$$

where we used the trace formulas of appendix B.

Even though the subset weights are free of the sign problem, the determinants in the original ensemble have a fluctuating sign. This can be well illustrated by computing the average phase of the fermion determinant in the phase-quenched ensemble, which is also the reweighting factor for phase-quenched reweighting (see section 4.2). For $N_f = 2$ this average phase can be computed analytically for arbitrary μ and m and is given by

$$\langle e^{2i\theta} \rangle_{\text{pq}} = \frac{Z^{(2)}}{Z^{(11^*)}}, \quad (4.8)$$

where $Z^{(2)}$ is given in (4.7) and $Z^{(11^*)} = \int dP |\det D|^2$ is the phase-quenched partition function, for which we find through group integration (using either (2.7) in combination with appendix A and B, or (2.4) in combination with the eigenvalue representation of the Polyakov loop in appendix D)

$$Z^{(11^*)} = (A^6 - 4A^4 + 5A^2 + 2) + (4A^3 - 4A) \cosh(\mu/T) + (2A^4 - 4A^2 + 4) \cosh(2\mu/T) \\ + (4A^3 - 8A) \cosh(3\mu/T) + 2A^2 \cosh(4\mu/T) + 2 \cosh(6\mu/T). \quad (4.9)$$

The average phase is shown in figure 6.

4.2 Larger N_f

For a larger number N_f of degenerate flavors the fermionic determinant is given by

$$\det^{N_f} D(P) = \sum_{q=-3N_f}^{3N_f} D_q^{(N_f)}(P) e^{q\mu/T}, \quad (4.10)$$

where the $D_q^{(N_f)}(P)$ are the canonical determinants for N_f flavors. We construct subsets Ω_P in exactly the same way as in eq. (4.2). In analogy to eq. (4.3) the subset weights are

$$\sigma(\Omega_P) = \frac{1}{6} \sum_{k=0}^2 \det^{N_f} D(P_k) + \text{c.c.}, \quad (4.11)$$

and the subset measurements are given by

$$\langle O \rangle_{\Omega_P} = \frac{1}{6\sigma(\Omega_P)} \sum_{k=0}^2 [\det^{N_f} D(P_k) O(P_k) + \det^{N_f} D(P_k^*) O(P_k^*)]. \quad (4.12)$$

After adding the determinants of the six configurations in the subset, we effectively project the determinants on the triality zero sector and obtain

$$\sigma(\Omega_P) = D_0^{(N_f)}(P) + \sum_{b=1}^{N_f-1} 2 \operatorname{Re} D_{3b}^{(N_f)}(P) \cosh(3b\mu/T) + 2 \cosh(3N_f\mu/T). \quad (4.13)$$

As in the case of $N_f = 2$, the subset weight was made real by adding the complex conjugate links to the subsets. However, there is no general argument for the positivity of these real subset weights for arbitrary number of flavors. In fact, we found that the subset weights are only strictly positive for small enough N_f . As we increase N_f the subset weights start to become negative. This first happens for $N_f \approx 5.11$ at $\mu \approx 0.96$ and for the subset containing the Polyakov loop with eigenvalues $(1, -1, -1)$. In figure 7 we show the value of the subset weight for this specific subset as a function of the chemical potential for different numbers of flavors in the massless case.⁸ As N_f is increased further, the regions in configuration space and chemical potential where the weights are negative slowly grow, see also figure 11 below.

Since for larger N_f the subset weights are not positive on the complete configuration space the subsets cannot be used in importance sampling and the subset method as such no longer works. Nonetheless, the subsets can still be useful in providing a good auxiliary system to simulate QCD₁ with N_f flavors using reweighting methods. In this case one generates relevant subsets according to the absolute value of the subset weights and absorbs the sign in the observable. The expectation value of an observable in the target ensemble is then given by the ratio of its signed expectation value and the average subset sign, both measured in the auxiliary ensemble, i.e.,

$$\langle O \rangle = \frac{\langle (\operatorname{sign} \sigma) \langle O \rangle_{\Omega_P} \rangle_{|\sigma|}}{\langle \operatorname{sign} \sigma \rangle_{|\sigma|}}. \quad (4.14)$$

This is the so-called sign-quenched reweighting scheme applied to the subset method.

Similar auxiliary systems can be considered for the original formulation of the partition function in terms of the SU(3) links, i.e., without subsets. Below, we compare the reweighting factors of the different approaches to investigate if the subset formulation brings an improvement to the sign problem. When comparing reweighting schemes it is customary

⁸For larger masses the threshold number of flavors will be higher.

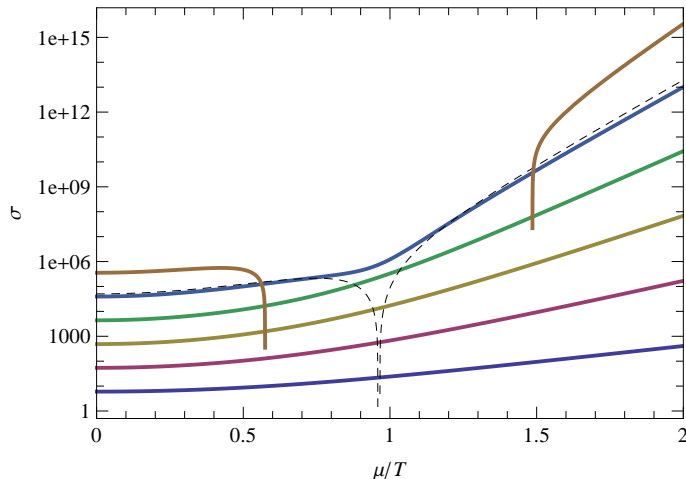


Figure 7. Subset weight in the massless case for Ω_P with $P = \text{diag}(1, -1, -1)$ as a function of μ/T for $N_f = 1, 2, \dots, 6$ (solid curves upwards) and a fictitious flavor number $N_f = 5.1102$ (dashed). As the weights are plotted on a logarithmic scale, the gap from $\mu/T = 0.57$ to 1.49 for $N_f = 6$ corresponds to negative weights.

to compare their reweighting factors, as these are good indicators of the severity of the sign problem and enter the computation of all expectation values.

In the subset formulation, the average reweighting factor in the sign-quenched reweighting scheme is the average subset sign in the sign-quenched ensemble,

$$R_{\text{sq}}^\sigma = \langle \text{sign } \sigma \rangle_{|\sigma|}. \quad (4.15)$$

As discussed above, a detailed investigation showed that all the subset weights are positive and the reweighting factor is exactly unity for $N_f \leq 5$. Clearly, no reweighting is necessary when using the subset method in this case. From $N_f = 6$ on, the average reweighting factor can become smaller than unity for some range of μ .

For the original link formulation of the partition function, several kinds of reweighting are possible, e.g., phase-quenched and sign-quenched reweighting. The average reweighting factors in these two schemes are given by the average phase factor and the average sign of the fermion determinant in the phase-quenched and sign-quenched ensembles, respectively,

$$R_{\text{pq}}^{\text{det}} = \langle e^{iN_f\theta} \rangle_{|\det^{N_f} D|}, \quad R_{\text{sq}}^{\text{det}} = \langle \text{sign}(\text{Re } \det^{N_f} D) \rangle_{|\text{Re } \det^{N_f} D|}, \quad (4.16)$$

where we used $\det D = |\det D|e^{i\theta}$. Note that $R_{\text{pq}}^{\text{det}}$ is the generalization of (4.8) to arbitrary N_f . The reweighting factors $R_{\text{pq}}^{\text{det}}$ and $R_{\text{sq}}^{\text{det}}$ can efficiently be computed numerically with the subset method as explained in ref. [12, section IV.C].

Let us first discuss phase-quenched reweighting in the link formulation. We derived analytical formulas for the average phase $R_{\text{pq}}^{\text{det}}$ in the phase-quenched ensemble, which can be expressed as the ratio of the unquenched and phase-quenched partition functions, see eq. (E.1). For even N_f the phase-quenched partition function can easily be computed, as it can be expressed as an integral over quarks and conjugate quarks. For odd N_f the

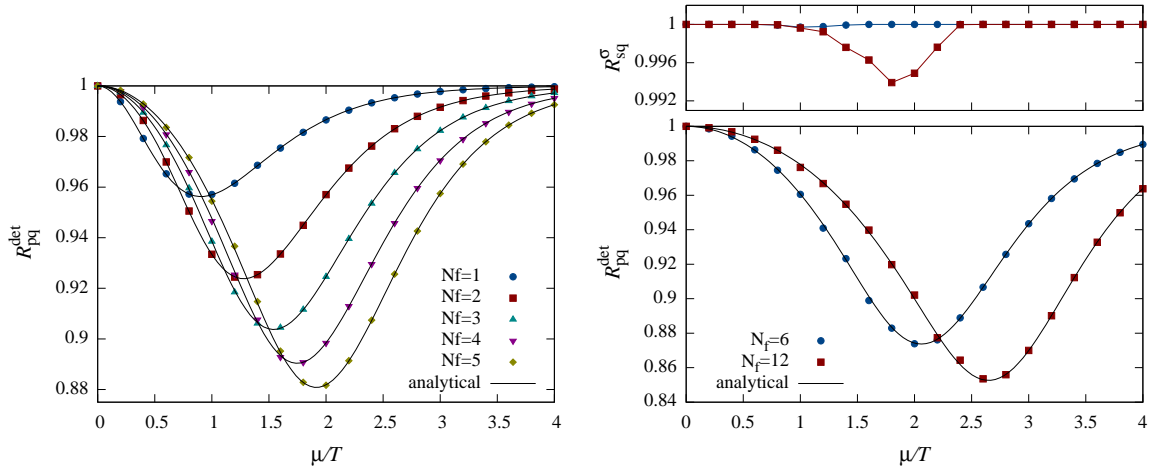


Figure 8. Average phase factor $R_{\text{pq}}^{\text{det}} = \langle e^{iN_f\theta} \rangle_{|\det^{N_f} D|}$ of the fermion determinant in the phase-quenched ensemble (at vanishing mass) for $N_f = 1, 2, 3, 4, 5$ (left) and $N_f = 6, 12$ (bottom right). The symbols represent the data measured with the subset method, the solid lines are the analytical results from appendix E. The narrow window at the top of the right panel shows the average sign $R_{\text{sq}}^{\sigma} = \langle \text{sign } \sigma \rangle_{|\sigma|}$ of the subset weights, illustrating that there is a mild sign problem for the subset method when $N_f \geq 6$.

computation is less trivial, as it involves an absolute value. Nevertheless, we were able to calculate analytical expressions for any N_f in the massless case, see appendix E. The numerical and analytical results for $R_{\text{pq}}^{\text{det}}$ are shown in figure 8. The numerical results were computed using the subset method. For $N_f = 1$ to 5 (left panel) the subset method can be used as is, but for $N_f = 6$ and $N_f = 12$ (right panel) a mild sign problem develops, and we use sign-quenched reweighting on the subset method, see (4.14). In this case we also show the average sign R_{sq}^{σ} of the subsets in the small top window. The sign problem in the subset method is clearly much milder than in the phase-quenched reweighting scheme using the $\text{SU}(3)$ links, as the average sign is much closer to one. Note that the minima in the bottom and top windows are shifted, meaning that the subset method has no sign problem where the sign problem of the phase-quenched reweighting scheme is maximal.

Let us now turn to sign-quenched reweighting in the link formulation, where the reweighting factor is the average sign of the real part of the determinant, rather than that of the subset weights, see eq. (4.16). While analytical results are not available for this average sign, numerical results can easily be obtained with the subset method and are shown in figure 9. Even though the average sign of the determinant is closer to one than its average phase [20], the subset reweighting scheme is still clearly superior.

Besides computing the average phase of the fermion determinant in the phase-quenched theory, which is relevant in the analysis of the phase-quenched reweighting scheme, one can also investigate this average phase in the full dynamical ensemble. An analytical expression for this quantity is currently not available, but numerical results can readily be obtained with the subset method. We show these results in figure 10. As expected, the average phase is smaller in the full theory than in the phase-quenched theory.

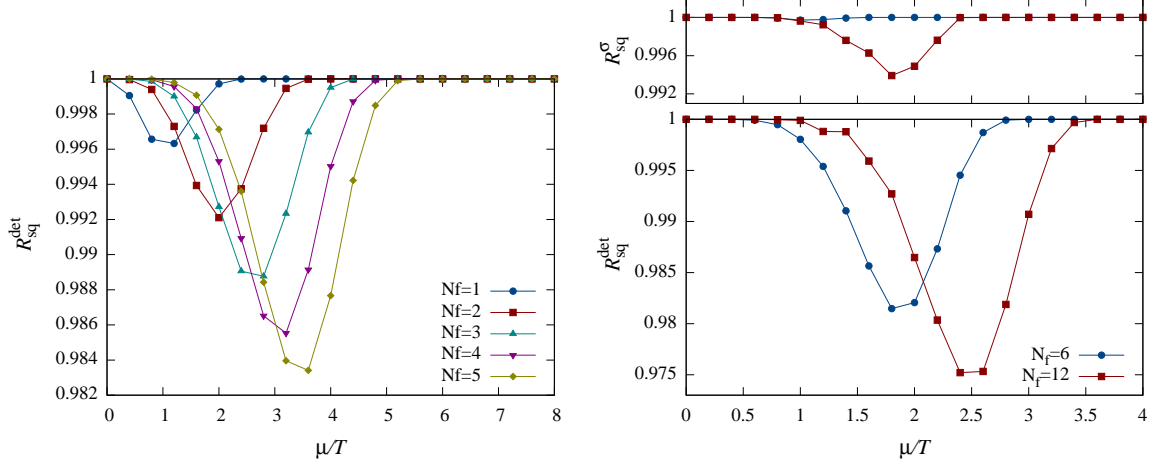


Figure 9. Average sign $R_{\text{sq}}^{\text{det}} = \langle \text{sign}(\text{Re det}^{N_f} D) \rangle_{|\text{Re det}^{N_f} D|}$ of the real part of the fermion determinant in the sign-quenched ensemble (at vanishing mass) for $N_f = 1, 2, 3, 4, 5$ (left) and $N_f = 6, 12$ (bottom right). Again, the narrow top window in the right panel shows the average sign of the subsets. The lines are drawn to guide the eye.

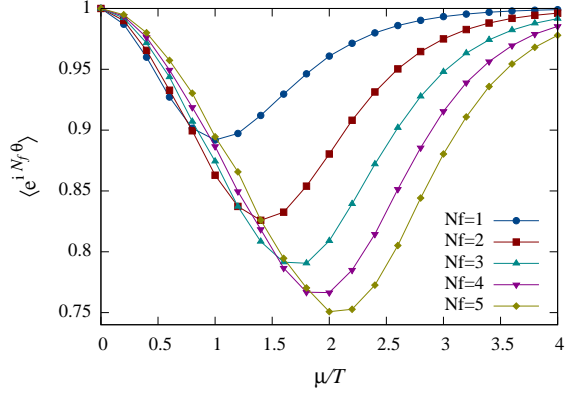


Figure 10. Average phase $\langle e^{i N_f \theta} \rangle$ of the fermion determinant in the unquenched ensemble as a function of μ/T for $N_f = 1, 2, 3, 4, 5$ with $m = 0$.

4.3 Extended subsets

Although the sign problem in the subset method is still mild for $N_f \geq 6$ and its severity only grows slowly with increasing N_f it would be preferable to avoid negative subset weights altogether. To achieve this we now extend the subset construction beyond the mere Z_3 rotations introduced in section 3.1.

Different routes can be taken. One could take advantage of the invariance of the Haar measure under rotation by a constant group element, which implies

$$\int dP f(P) = \int dP f(GP) \quad (4.17)$$

for arbitrary $G \in \text{SU}(3)$. The QCD_1 partition function can then be rewritten as an integral over extended subsets $\Omega_P^G = \Omega_P \cup \Omega_{GP}$, where Ω_P and Ω_{GP} are constructed following

eq. (4.2).⁹ The sign problem would then be solved if a constant group element G could be found for which the sum of determinants of the configurations in Ω_P^G is nonnegative. However, it is not clear how to find such a G as it requires an analysis of the landscape of the subset weight $\sigma(\Omega_P)$ in the full 8-dimensional parameter space of P .

What seems like a more feasible task is to analyze the landscape of the subset weight in the eigenvalue representation $P = \text{diag}(e^{i\theta_1}, e^{i\theta_2}, e^{-i\theta_1-i\theta_2})$, see appendix D, and try to find a constant G of the form $G = \text{diag}(e^{i\alpha}, e^{i\beta}, e^{-i\alpha-i\beta})$ to solve the sign problem. To see why this is sensible, first note that any P can be diagonalized as

$$P = U \text{diag}(e^{i\theta_1}, e^{i\theta_2}, e^{-i\theta_1-i\theta_2}) U^\dagger. \quad (4.18)$$

We now shift the angles,

$$\theta_1 \rightarrow \theta'_1 = \theta_1 + \alpha, \quad \theta_2 \rightarrow \theta'_2 = \theta_2 + \beta, \quad (4.19)$$

and create a “rotated” link

$$P' = R(P, G) \equiv U \text{diag}(e^{i\theta'_1}, e^{i\theta'_2}, e^{-i\theta'_1-i\theta'_2}) U^\dagger \quad (4.20)$$

that has the same eigenvectors as P . It is then straightforward to show that the partition function can be rewritten as

$$\begin{aligned} Z^{(N_f)} &= \frac{1}{2} \left[\int dP \sigma(\Omega_P) + \int dP' \sigma(\Omega_{P'}) \right] \\ &= \frac{1}{2} \int dP \left[\sigma(\Omega_P) + \frac{J(\theta'_1, \theta'_2)}{J(\theta_1, \theta_2)} \sigma(\Omega_{P'}) \right], \end{aligned} \quad (4.21)$$

where J is given in (D.3). The contribution of P' is rescaled by the ratio of the Jacobians of P' and P . Now note that in QCD₁ the subset weight is a class function, i.e., it only depends on θ_1 and θ_2 , rather than the full P . We can therefore rewrite (4.21) as

$$Z^{(N_f)} = \frac{1}{2} \int J(\theta_1, \theta_2) d\theta_1 d\theta_2 \left[\sigma(\Omega_P) + \frac{J(\theta'_1, \theta'_2)}{J(\theta_1, \theta_2)} \sigma(\Omega_{P'}) \right]. \quad (4.22)$$

For observables that are also class functions, it suffices to generate diagonal Polyakov loops according to the weight $J(\theta_1, \theta_2)$. We numerically verified the validity of both (4.21) and (4.22) by computing observables in both formulations.

The extension of the original Z_3 subset by an additional Z_3 subset constructed with a single G does not obey the symmetry of $\text{tr} P$ under permutations of the angles θ_1 , θ_2 , and $\theta_3 = -\theta_1 - \theta_2$. Therefore we consider a larger extension of the subset using six rotations $\mathcal{G} = \{G_1, \dots, G_6\}$ with all possible permutations of α and β over the three eigenvalues, i.e.,

$$\begin{aligned} G_1 &= \text{diag}(e^{i\alpha}, e^{i\beta}, e^{-i\alpha-i\beta}), & G_2 &= \text{diag}(e^{-i\alpha-i\beta}, e^{i\alpha}, e^{i\beta}), & G_3 &= \text{diag}(e^{i\beta}, e^{-i\alpha-i\beta}, e^{i\alpha}), \\ G_4 &= \text{diag}(e^{i\beta}, e^{i\alpha}, e^{-i\alpha-i\beta}), & G_5 &= \text{diag}(e^{-i\alpha-i\beta}, e^{i\beta}, e^{i\alpha}), & G_6 &= \text{diag}(e^{i\alpha}, e^{-i\alpha-i\beta}, e^{i\beta}). \end{aligned} \quad (4.23)$$

⁹This construction can be generalized to more than one group element, i.e., $\Omega_P^{\{G\}} = \Omega_P \cup \Omega_{G_1 P} \cup \Omega_{G_2 P} \cup \dots$

If $\alpha = \beta$, $-\beta/2$, or -2β the number of permutations is reduced to three. The extended subsets, containing 21 configurations and their complex conjugates, are defined as

$$\Omega_P^{\text{ext}} = \bigcup_{i=0}^6 \Omega_{P^{(i)}} \quad (4.24)$$

with $P^{(i)} = R(P, G_i)$ using the rotations (4.20), and $G_0 = \mathbb{1}$. The QCD₁ partition function can then be rewritten as

$$Z^{(N_f)} = \int dP \sigma_P^{\text{ext}} \quad (4.25)$$

with extended subset weights

$$\sigma_P^{\text{ext}} = \frac{1}{7} \sum_{i=0}^6 \frac{J(P^{(i)})}{J(P)} \sigma(\Omega_{P^{(i)}}), \quad (4.26)$$

where $J(P) = J(\theta_1, \theta_2)$ and $\sigma(\Omega_{P^{(i)}})$ is the Z_3 subset weight defined in eq. (4.11). The subset measurement on the extended subset is defined as

$$\langle O \rangle_{\Omega_P^{\text{ext}}} = \frac{1}{7\sigma_P^{\text{ext}}} \sum_{i=0}^6 \frac{J(P^{(i)})}{J(P)} \sigma(\Omega_{P^{(i)}}) \langle O \rangle_{\Omega_{P^{(i)}}} \quad (4.27)$$

with the measurement on a single Z_3 subset as in (4.12). With this definition, (3.4) and (3.6) straightforwardly generalize to extended subsets (and any N_f).

In figure 11 we give an example of the effect of the rotations G_i on the extended subset weight for $N_f = 24$ and $\mu/T = 2.6$ (top) and $\mu/T = 1.3$ (bottom).¹⁰ Note that the sign problem is maximal for $\mu/T = 2.6$, see figure 12 below. In the left panels we show the logarithm of $J(P)$ times the subset weights (4.11) for the original Z_3 subsets. We clearly see regions where the subset weights are negative. The Swiss-cheese pattern is fairly rigid in the sense that the location of the holes seems independent of N_f and μ ; only their sizes change, and occasionally some isle-formation is observed inside the holes.¹¹ From the location of the holes we can make an educated guess for good shifts α and β for the construction of the rotations G_i . In the right panels of figure 11 we show the logarithm of $J(P)$ times the subset weights (4.26) for extended subsets with α and β given in the caption. The extended subsets solve the sign problem in the illustrated cases. For large N_f there does not seem to be a single choice \mathcal{G} of rotations that solves the sign problem over the complete μ range, and one should adapt \mathcal{G} to the value of μ .¹²

¹⁰Note that allowing θ_1 and θ_2 to range from 0 to 2π leads to a mosaic of six replicated regions, caused by the permutation symmetries of the subset weights. The fundamental region can, for example, be defined as the triangle with corners $(\theta_1, \theta_2) \in \{(2\pi/3, 2\pi/3), (4\pi/3, 4\pi/3), (2\pi, 0)\}$ delimited by the lines $\theta_2 = \theta_1$, $2\theta_2 + \theta_1 = 2\pi$, and $\theta_2 + 2\theta_1 = 4\pi$.

¹¹The average sign R_{sq}^{σ} equals 0.98836 for $\mu/T = 2.6$ and 0.99988 for $\mu/T = 1.3$, i.e., the sign problem is much milder in the latter case although the holes are of similar size. In this case the absolute value of the weights in the negative region is very small compared to the positive region.

¹²Even if we have picked a \mathcal{G} that does not solve the sign problem completely the numerical simulations can simply switch to sign-quenched reweighting if negative weights occur. The average sign can be used to monitor the remaining (very mild) sign problem.

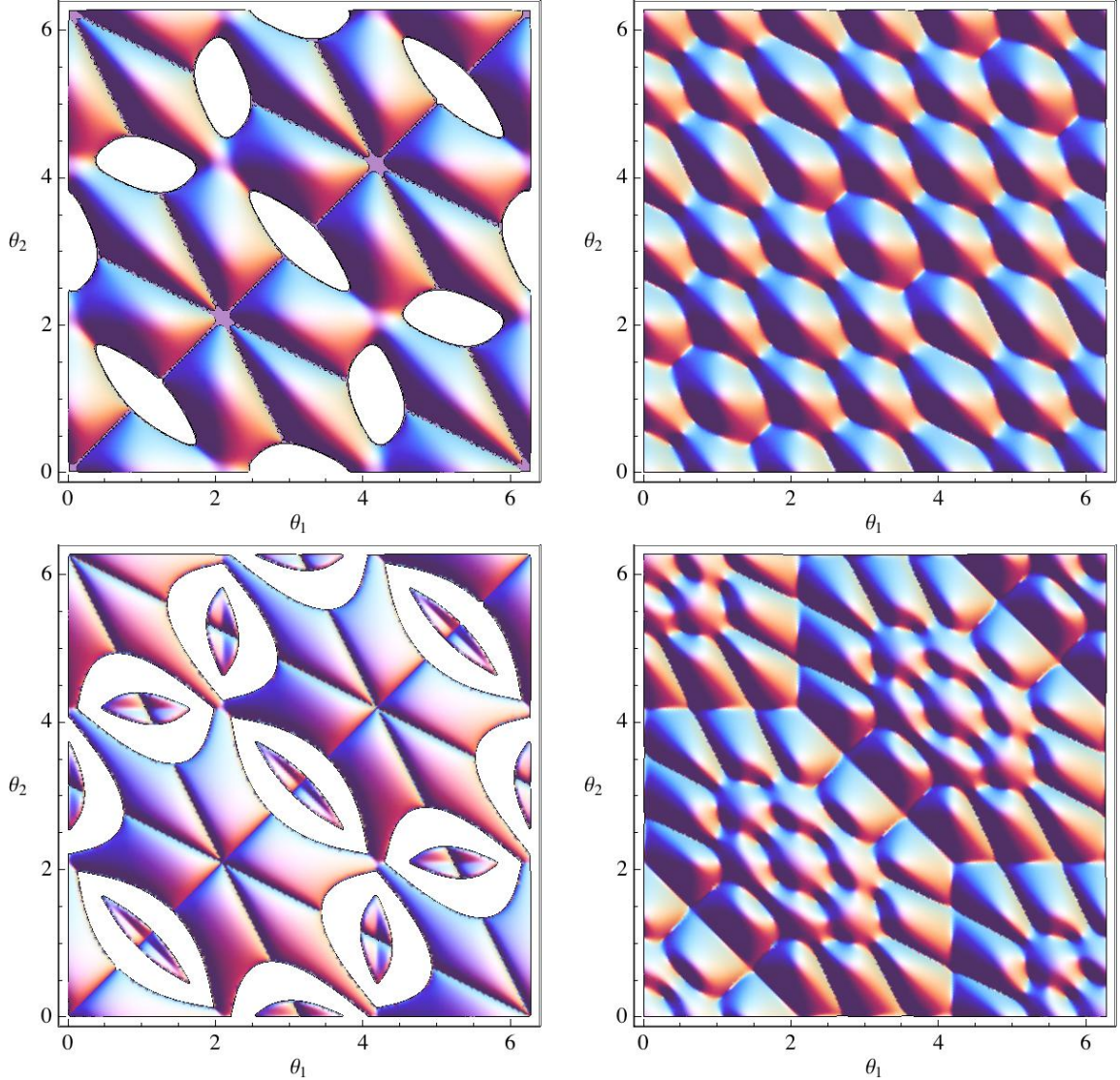


Figure 11. Plot of $\log[J(P) \sigma(\Omega_P)]$ (left) and $\log[J(P) \sigma_P^{\text{ext}}]$ (right) as a function of the Polyakov loop angles for $\mu/T = 2.6$ (top) and 1.3 (bottom), both for $N_f = 24$ and $m = 0$. The holes in the surface correspond to negative weights on the logarithmic scale. On the left, the weights (4.11) of the original Z_3 subsets exhibit a clear sign problem. On the right, the weights (4.26) of the extended subsets were generated using $\alpha = -\beta = \pi/3$ for $\mu/T = 2.6$ and $\alpha = -\beta = \pi/4$ for $\mu/T = 1.3$, respectively. We observe that the sign problem is eliminated for these parameter values.

As a final illustration of the extended subsets we compare the average sign of the original Z_3 subset weight to the average sign of the extended subsets with a fixed choice of $\alpha = -\beta = \pi/3$ as a function of μ/T for $N_f = 12, 24, 48$ in figure 12. The Z_3 subsets have a mild sign problem, which is completely eliminated by the extended subsets for $N_f = 12$ and eliminated for almost all values of μ/T for $N_f = 24$ and 48 (for the fixed choice of α and β).

We should remark that our subset solution to the sign problem in QCD_1 does not immediately yield a solution to the exponential sign problem occurring in higher dimensions

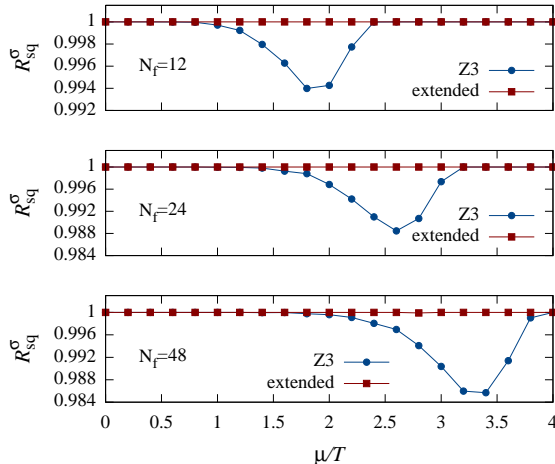


Figure 12. Comparison of the average sign R_{sq}^σ of the subset weight for the original Z_3 subsets and for the extended subsets, with $N_f = 12, 24, 48$, $m = 0$, and fixed $\alpha = -\beta = \pi/3$. The occasional tiny deviations from 1 for the extended subsets are hardly visible.

($d > 1$), even if the resulting subset weights are positive. Indeed, if we assume naively that each temporal link requires the construction of its own “one-link subset” with N elements, we would have N^V elements per “lattice subset” for a d -dimensional lattice with volume $V = N_t \times N_s^{d-1}$. In that case the number of elements, and thus the computation time, grows exponentially with the volume. To solve the exponential sign problem, a subset solution on a higher-dimensional lattice should have a *collective* nature, where subsets are formed using collective rather than individual transformations of the links on different sites such that the higher-dimensional subset is not a direct product of subsets on each lattice site.

5 Summary

In this paper we presented a subset method to eliminate the sign problem in dynamical simulations of QCD in 0+1 dimensions at nonzero chemical potential. The $SU(3)$ links are gathered into subsets, each containing three links that are related by a Z_3 rotation. We showed that the sum of fermion determinants of the three configurations in any such subset is real and positive for $N_f = 1$. For $N_f = 2, \dots, 5$ the real parts of the subset weights are still positive. Their imaginary parts, which can be nonvanishing, are removed by adding the complex conjugate links to the subsets such that the subsets contain six links in total. The positive subset weights can then be used to generate Markov chains of relevant subsets using importance sampling. The method was illustrated by computing the quark number density, the chiral condensate, and the Polyakov loop numerically and comparing the data with analytical results, some of which were derived for the first time in this paper.

For $N_f \geq 6$ the subset weights are no longer generically positive. However, their average sign is still very close to unity so that reweighting methods can be used. We showed that sign-quenched reweighting in the subset ensemble is much more efficient than the standard phase-quenched or sign-quenched reweighting on the individual determinants.

Finally, we constructed extended subsets by performing additional $SU(3)$ rotations. If chosen judiciously, these extended subsets have positive weights even for $N_f \geq 6$.

Although we managed to get rid of the non-positivity of the weights in the partition function by gathering configurations into subsets, we cannot claim to have solved an exponential sign problem. A creative adaptation of the subset construction to higher dimensions is needed to arrive at such a solution.

Acknowledgments

We thank Christof Gattringer and Kim Splittorff for useful discussions. This work was supported in part by the DFG collaborative research center SFB/TRR-55, by DFG grant BR 2872/4-2, and by the Alexander von Humboldt Foundation.

A One-flavor determinant

In this appendix we compute the coefficients D_q in expression (2.7) for the $N_f = 1$ determinant. We start with eq. (2.4) without the prefactor $1/2^{3N_t}$,

$$\det D = \det(e^\mu P + e^{-\mu} P^\dagger + A \mathbb{1}_3), \quad (\text{A.1})$$

where for simplicity of notation we replaced $\mu/T \rightarrow \mu$. This determinant can be computed explicitly using the formula for 3×3 determinants in terms of traces,

$$6 \det M = (\text{tr } M)^3 - 3 \text{tr } M \text{tr } M^2 + 2 \text{tr } M^3, \quad (\text{A.2})$$

where $M = e^\mu P + e^{-\mu} P^\dagger + A \mathbb{1}_3$ in this case. Using the traces

$$\text{tr } M = e^\mu \text{tr } P + 3A + e^{-\mu} \text{tr } P^\dagger, \quad (\text{A.3})$$

$$\text{tr } M^2 = e^{2\mu} \text{tr } P^2 + e^\mu 2A \text{tr } P + 3A^2 + 6 + e^{-\mu} 2A \text{tr } P^\dagger + e^{-2\mu} \text{tr } P^{\dagger 2}, \quad (\text{A.4})$$

$$\begin{aligned} \text{tr } M^3 = & e^{3\mu} \text{tr } P^3 + e^{2\mu} 3A \text{tr } P^2 + e^\mu 3(A^2 + 1) \text{tr } P + 3A^3 + 18A \\ & + e^{-\mu} 3(A^2 + 1) \text{tr } P^\dagger + e^{-2\mu} 3A \text{tr } P^{\dagger 2} + e^{-3\mu} \text{tr } P^{\dagger 3} \end{aligned} \quad (\text{A.5})$$

we find

$$\det D = \sum_{q=-3}^3 D_q e^{q\mu} \quad (\text{A.6})$$

with coefficients

$$D_0(P) = A^3 - 3A + A |\text{tr } P|^2, \quad (\text{A.7})$$

$$D_1(P) = D_{-1}(P)^* = (A^2 - 2) \text{tr } P + (\text{tr } P^\dagger)^2, \quad (\text{A.8})$$

$$D_2(P) = D_{-2}(P)^* = A \text{tr } P^\dagger, \quad (\text{A.9})$$

$$D_3(P) = D_{-3}(P)^* = 1, \quad (\text{A.10})$$

where we also used $6 \det P = (\text{tr } P)^3 - 3 \text{tr } P \text{tr } P^2 + 2 \text{tr } P^3 = 6$ as $P \in SU(3)$, and $\text{tr } P^2 = (\text{tr } P)^2 - 2 \text{tr } P^\dagger$, which follows, e.g., from (D.1).

B Some integrals of traces

In our calculations we need some integrals of powers of traces of the (anti-) Polyakov loop. To compute them, we construct the tensor product of k copies of the fundamental and ℓ copies of the anti-fundamental representation of $SU(3)$ and decompose the product into irreducible representations,

$$t = \underbrace{3 \otimes \cdots \otimes 3}_{k \text{ times}} \otimes \underbrace{\bar{3} \otimes \cdots \otimes \bar{3}}_{\ell \text{ times}} = \bigoplus_i n_i r_i, \quad (\text{B.1})$$

where t stands for the tensor product representation and n_i is the multiplicity with which the irreducible representation r_i occurs in the decomposition. We now take the trace of P in the tensor product representation and obtain

$$\int dP \operatorname{tr} P^{(t)} = \int dP (\operatorname{tr} P)^k (\operatorname{tr} P^\dagger)^\ell = \sum_i n_i \underbrace{\int dP \operatorname{tr} P^{(r_i)}}_{= \delta_{i0}} = n_0, \quad (\text{B.2})$$

where r_0 is the trivial representation and the last integral follows from the orthonormality relations of the group characters. Note that (B.2) is only nonzero if $(k - \ell) \bmod 3 = 0$. By suitable choices of k and ℓ we obtain

$$\int dP |\operatorname{tr} P|^2 = 1 \quad \text{from} \quad 3 \otimes \bar{3} = 8 \oplus 1, \quad (\text{B.3})$$

$$\int dP (\operatorname{tr} P)^3 = 1 \quad \text{from} \quad 3 \otimes 3 \otimes 3 = 10 \oplus 8 \oplus 8 \oplus 1, \quad (\text{B.4})$$

$$\int dP |\operatorname{tr} P|^4 = 2 \quad \text{from} \quad 3 \otimes \bar{3} \otimes 3 \otimes \bar{3} = 27 \oplus 10 \oplus \bar{10} \oplus 8 \oplus 8 \oplus 8 \oplus 8 \oplus 1 \oplus 1. \quad (\text{B.5})$$

Alternatively, we could use the eigenvalue representation of P (see appendix D) and integrate over θ_1 and θ_2 .

C Relation between quark number density and Polyakov loop

In this appendix we consider a general number N_f of flavors. The quark number density is

$$n = \frac{T}{N_f} \frac{\partial \log Z^{(N_f)}}{\partial \mu} = \frac{1}{Z^{(N_f)}} \int dP \det^{N_f} D \operatorname{tr} \gamma, \quad (\text{C.1})$$

where γ is defined as

$$\gamma = \frac{p - 1/p}{p + 1/p + 2 \cosh(\mu_c)} \quad (\text{C.2})$$

with $p = e^\mu P$. Here and below we have replaced $\mu_c/T \rightarrow \mu_c$ and $\mu/T \rightarrow \mu$ for simplicity of notation. We also assume $\mu_c \geq 0$ without loss of generality. After factorizing the denominator of γ and performing a partial fraction expansion we find

$$\begin{aligned} \gamma &= \frac{e^{\pm \mu_c} (p - 1/p)}{(1 + e^{\pm \mu_c} p)(1 + e^{\pm \mu_c} / p)} \\ &= \frac{1}{1 + e^{\pm \mu_c - \mu} P^\dagger} - \frac{1}{1 + e^{\pm \mu_c + \mu} P}. \end{aligned} \quad (\text{C.3})$$

	(a) $\mu < -\mu_c$	(b) $-\mu_c < \mu < \mu_c$	(c) $\mu_c < \mu$
$+\mu_c - \mu$	+	+	-
$+\mu_c + \mu$	-	+	+
$-\mu_c - \mu$	+	-	-
$-\mu_c + \mu$	-	-	+

Table 1. Signs of the exponents $\pm\mu_c \pm \mu$ in (C.3) for $\mu < -\mu_c$, $-\mu_c < \mu < \mu_c$, and $\mu_c < \mu$.

Although it is not obvious from the final expression, (C.3) is valid for either sign in front of μ_c . However, the same sign has to be chosen for all occurrences of μ_c . Each of the two terms in (C.3) can be considered as the result of a geometric series. When expanding these series care has to be taken to ensure their convergence. As the eigenvalues of P all have unit magnitude, the convergence requires the exponents in (C.3) to be negative. The signs of these exponents depend on the relative values of μ and μ_c , for which we distinguish three cases that are detailed in table 1. From the table we read off that the following expansion is valid for $-\mu_c < \mu < \mu_c$:

$$\gamma = \sum_{\omega=1}^{\infty} (-)^{\omega} \left(e^{\omega(-\mu_c-\mu)} (P^\dagger)^\omega - e^{\omega(-\mu_c+\mu)} P^\omega \right). \quad (\text{C.4})$$

To expand (C.3) in a convergent series for $\mu < -\mu_c$ we first extract $e^{\pm\mu_c-\mu} P^\dagger$ from the denominator of the first term and find

$$\gamma = \frac{e^{\mp\mu_c+\mu} P}{1 + e^{\mp\mu_c+\mu} P} - \frac{1}{1 + e^{\pm\mu_c+\mu} P} = -1 - 2 \sum_{\omega=1}^{\infty} (-)^{\omega} \cosh(\omega\mu_c) e^{\omega\mu} P^\omega. \quad (\text{C.5})$$

Analogously, the series for $\mu_c < \mu$ is given by

$$\gamma = \frac{1}{1 + e^{\pm\mu_c-\mu} P^\dagger} - \frac{e^{\mp\mu_c-\mu} P^\dagger}{1 + e^{\mp\mu_c-\mu} P^\dagger} = 1 + 2 \sum_{\omega=1}^{\infty} (-)^{\omega} \cosh(\omega\mu_c) e^{-\omega\mu} (P^\dagger)^\omega. \quad (\text{C.6})$$

From the eigenvalue representation of the Polyakov loop we can show (by counting powers of $e^{i\theta_1}$ and $e^{i\theta_2}$) that the expectation value of $\text{tr} P^{\pm\omega}$ is zero for $|\omega| > 2N_f + 3$ such that substitution of eqs. (C.4)–(C.6) in eq. (C.2) yields

$$n = \begin{cases} -3 - 2 \sum_{\omega=1}^{2N_f+3} (-)^{\omega} \cosh(\omega\mu_c) e^{\omega\mu} \langle \text{tr} P^\omega \rangle, & \mu < -\mu_c, \\ \sum_{\omega=1}^{2N_f+3} (-)^{\omega} e^{-\omega\mu_c} \left(e^{-\omega\mu} \langle \text{tr}(P^\dagger)^\omega \rangle - e^{\omega\mu} \langle \text{tr} P^\omega \rangle \right), & -\mu_c < \mu < \mu_c, \\ 3 + 2 \sum_{\omega=1}^{2N_f+3} (-)^{\omega} \cosh(\omega\mu_c) e^{-\omega\mu} \langle \text{tr}(P^\dagger)^\omega \rangle, & \mu_c < \mu. \end{cases} \quad (\text{C.7})$$

We conjecture that all three finite sums are identical over the complete μ -range, which we explicitly verified for $N_f = 1$ and $N_f = 2$. If this is the case, a somewhat more symmetric equation is found by combining the first and third formula,

$$n = \sum_{\omega=1}^{2N_f+3} (-)^{\omega} \cosh(\omega\mu_c) \left(e^{-\omega\mu} \langle \text{tr}(P^\dagger)^\omega \rangle - e^{\omega\mu} \langle \text{tr} P^\omega \rangle \right). \quad (\text{C.8})$$

Note that even though the finite sums (C.7) stand out by the simplicity of their coefficients (for arbitrary N_f), shorter sums involving lower winding numbers ω , but with typically more complicated coefficients, also exist. For instance, for $N_f = 1$ a simpler result is given in (3.24), while for $N_f = 2$ we found

$$n_{N_f=2} = \frac{3}{2 + \cosh 2\mu_c} \left[\cosh \mu_c \langle e^\mu \text{tr} P - e^{-\mu} \text{tr} P^\dagger \rangle + \frac{1}{4} \langle e^{2\mu} \text{tr} P^2 - e^{-2\mu} \text{tr}(P^\dagger)^2 \rangle \right]. \quad (\text{C.9})$$

These short sums reduce the maximal winding number for $N_f = 1$ from 5 to 1 and for $N_f = 2$ from 7 to 2. Similar sums can be derived for larger N_f , but no simple formula was found for their coefficients.

D SU(3) eigenvalue representation

It is often convenient to work in the eigenvalue representation of the Polyakov loop. The latter is diagonalized as $P = U\Lambda U^\dagger$ with

$$\Lambda = \text{diag}(e^{i\theta_1}, e^{i\theta_2}, e^{-i\theta_1 - i\theta_2}), \quad (\text{D.1})$$

where $\theta_1, \theta_2 \in [0, 2\pi]$ and $U \in \text{U}(3)/\text{U}(1)^{\otimes 3}$. The Haar measure is then given by

$$dP = J(\theta_1, \theta_2) d\theta_1 d\theta_2 dU, \quad (\text{D.2})$$

where dU is the normalized measure of $\text{U}(3)/\text{U}(1)^{\otimes 3}$ and the Jacobian is a Vandermonde determinant that only depends on θ_1 and θ_2 . It is given by

$$\begin{aligned} J(\theta_1, \theta_2) &= \frac{1}{24\pi^2} |(e^{i\theta_1} - e^{i\theta_2})(e^{i\theta_1} - e^{-i\theta_1 - i\theta_2})(e^{i\theta_2} - e^{-i\theta_1 - i\theta_2})|^2 \\ &= \frac{8}{3\pi^2} \sin^2 \frac{\theta_1 - \theta_2}{2} \sin^2 \frac{2\theta_1 + \theta_2}{2} \sin^2 \frac{\theta_1 + 2\theta_2}{2}, \end{aligned} \quad (\text{D.3})$$

where the prefactor ensures $\int dP = 1$.

E Average phase in the phase-quenched theory

In this section we compute the average phase of the N_f -flavor determinant in the phase-quenched theory. This average phase factor can be written as the ratio of the unquenched and phase-quenched partition functions,

$$\langle e^{iN_f\theta} \rangle_{\text{pq}} = \frac{\langle (\det D)^{N_f} \rangle_{N_f=0}}{\langle |\det D|^{N_f} \rangle_{N_f=0}}. \quad (\text{E.1})$$

For odd N_f it is difficult to compute the denominator on the RHS since it involves square roots. In the eigenvalue representation of P the fermion determinant is given by

$$\det D = \prod_{k=1}^3 (A + e^{\mu + i\theta_k} + e^{-\mu - i\theta_k}) \quad \text{with} \quad \theta_3 = -\theta_1 - \theta_2, \quad (\text{E.2})$$

where we again replaced $\mu/T \rightarrow \mu$ for simplicity of notation. For a single angle we have

$$\begin{aligned} |A + e^{\mu+i\theta} + e^{-\mu-i\theta}| &= |A + 2 \cosh \mu \cos \theta + 2i \sinh \mu \sin \theta| \\ &= [(2 \cosh \mu + A \cos \theta)^2 + (A^2 - 4) \sin^2 \theta]^{1/2}. \end{aligned} \quad (\text{E.3})$$

This expression will be raised to the power N_f so that the square root disappears for even N_f . For odd N_f the square root cannot be taken unless $A = 2$, which corresponds to the chiral limit. For simplicity we now consider only this limit, in which

$$|A + e^{\mu+i\theta} + e^{-\mu-i\theta}| = 2(\cosh \mu + \cos \theta). \quad (\text{E.4})$$

We can then compute $\langle |\det D|^{N_f} \rangle_0$ by integrating over θ_1 and θ_2 ,

$$\begin{aligned} \langle |\det D|^{N_f} \rangle_0 &= 8^{N_f} \int_0^{2\pi} \int_0^{2\pi} J(\theta_1, \theta_2) d\theta_1 d\theta_2 \\ &\times [(\cosh \mu + \cos \theta_1)(\cosh \mu + \cos \theta_2)(\cosh \mu + \cos(\theta_1 + \theta_2))]^{N_f}. \end{aligned} \quad (\text{E.5})$$

In the following we state some explicit results for $\langle (\det D)^{N_f} \rangle_0$ and $\langle |\det D|^{N_f} \rangle_0$ in the chiral limit that have been used in figure 8. For even N_f these results can easily be generalized to $A > 2$, while the possibility of such a generalization is not obvious for odd N_f .

$$\begin{aligned} \langle \det D \rangle_0 &= 4 + 2 \cosh(3\mu), \\ \langle |\det D| \rangle_0 &= 2 + 2 \cosh \mu + 2 \cosh(3\mu), \\ \langle (\det D)^2 \rangle_0 &= 50 + 40 \cosh(3\mu) + 2 \cosh(6\mu), \\ \langle |\det D|^2 \rangle_0 &= 22 + 24 \cosh \mu + 20 \cosh(2\mu) + 16 \cosh(3\mu) + 8 \cosh(4\mu) + 2 \cosh(6\mu), \\ \langle (\det D)^3 \rangle_0 &= 980 + 980 \cosh(3\mu) + 112 \cosh(6\mu) + 2 \cosh(9\mu), \\ \langle |\det D|^3 \rangle_0 &= 330 + 612 \cosh \mu + 432 \cosh(2\mu) + 370 \cosh(3\mu) + 180 \cosh(4\mu) \\ &\quad + 90 \cosh(5\mu) + 40 \cosh(6\mu) + 18 \cosh(7\mu) + 2 \cosh(9\mu), \\ \langle (\det D)^4 \rangle_0 &= 24696 + 28224 \cosh(3\mu) + 5040 \cosh(6\mu) + 240 \cosh(9\mu) + 2 \cosh(12\mu), \\ \langle |\det D|^4 \rangle_0 &= 8434 + 15040 \cosh \mu + 12904 \cosh(2\mu) + 9360 \cosh(3\mu) + 6262 \cosh(4\mu) \\ &\quad + 3264 \cosh(5\mu) + 1832 \cosh(6\mu) + 720 \cosh(7\mu) + 272 \cosh(8\mu) \\ &\quad + 80 \cosh(9\mu) + 32 \cosh(10\mu) + 2 \cosh(12\mu), \\ \langle (\det D)^5 \rangle_0 &= 731808 + 914760 \cosh(3\mu) + 217800 \cosh(6\mu) + 18150 \cosh(9\mu) \\ &\quad + 440 \cosh(12\mu) + 2 \cosh(15\mu), \\ \langle |\det D|^5 \rangle_0 &= 241752 + 464250 \cosh \mu + 390980 \cosh(2\mu) + 308390 \cosh(3\mu) \\ &\quad + 209600 \cosh(4\mu) + 132706 \cosh(5\mu) + 72800 \cosh(6\mu) \\ &\quad + 37450 \cosh(7\mu) + 15540 \cosh(8\mu) + 6550 \cosh(9\mu) + 2100 \cosh(10\mu) \\ &\quad + 650 \cosh(11\mu) + 140 \cosh(12\mu) + 50 \cosh(13\mu) + 2 \cosh(15\mu), \\ \langle (\det D)^6 \rangle_0 &= 24293412 + 32391216 \cosh(3\mu) + 9447438 \cosh(6\mu) + 1145144 \cosh(9\mu) \\ &\quad + 52052 \cosh(12\mu) + 728 \cosh(15\mu) + 2 \cosh(18\mu), \\ \langle |\det D|^6 \rangle_0 &= 8100348 + 15385104 \cosh \mu + 13537836 \cosh(2\mu) + 10757544 \cosh(3\mu) \end{aligned}$$

$$\begin{aligned}
& + 7905636 \cosh(4\mu) + 5210856 \cosh(5\mu) + 3192856 \cosh(6\mu) \\
& + 1735920 \cosh(7\mu) + 875016 \cosh(8\mu) + 386960 \cosh(9\mu) \\
& + 160974 \cosh(10\mu) + 55440 \cosh(11\mu) + 18832 \cosh(12\mu) + 5040 \cosh(13\mu) \\
& + 1332 \cosh(14\mu) + 224 \cosh(15\mu) + 72 \cosh(16\mu) + 2 \cosh(18\mu), \\
\langle (\det D)^{12} \rangle_0 & = 114801908084920000 + 183683052935872000 \cosh(3\mu) \\
& + 93809559177963200 \cosh(6\mu) + 30350151498752800 \cosh(9\mu) \\
& + 6136979163350750 \cosh(12\mu) + 759997419610000 \cosh(15\mu) \\
& + 55999809866000 \cosh(18\mu) + 2357886731200 \cosh(21\mu) \\
& + 53588334800 \cosh(24\mu) + 605176000 \cosh(27\mu) \\
& + 2990000 \cosh(30\mu) + 5200 \cosh(33\mu) + 2 \cosh(36\mu), \\
\langle |\det D|^{12} \rangle_0 & = 38228935544196544 + 74588093808767136 \cosh \mu \\
& + 69256334029071024 \cosh(2\mu) + 61191395371363712 \cosh(3\mu) \\
& + 51446943705501036 \cosh(4\mu) + 41144000777152416 \cosh(5\mu) \\
& + 31295396191130192 \cosh(6\mu) + 22628417756712768 \cosh(7\mu) \\
& + 15550003072387944 \cosh(8\mu) + 10148555203557056 \cosh(9\mu) \\
& + 6288313704156072 \cosh(10\mu) + 3695893600669920 \cosh(11\mu) \\
& + 2059587221609088 \cosh(12\mu) + 1086906242675088 \cosh(13\mu) \\
& + 542935067374728 \cosh(14\mu) + 256303460885472 \cosh(15\mu) \\
& + 114289127660268 \cosh(16\mu) + 48034918945728 \cosh(17\mu) \\
& + 19022357453088 \cosh(18\mu) + 7076078360208 \cosh(19\mu) \\
& + 2472827265612 \cosh(20\mu) + 808058178928 \cosh(21\mu) \\
& + 247249295568 \cosh(22\mu) + 70294375008 \cosh(23\mu) \\
& + 18651768124 \cosh(24\mu) + 4554250272 \cosh(25\mu) + 1036301112 \cosh(26\mu) \\
& + 213188976 \cosh(27\mu) + 41112918 \cosh(28\mu) + 6918912 \cosh(29\mu) \\
& + 1120264 \cosh(30\mu) + 144144 \cosh(31\mu) + 20880 \cosh(32\mu) \\
& + 1456 \cosh(33\mu) + 288 \cosh(34\mu) + 2 \cosh(36\mu).
\end{aligned}$$

References

- [1] N. Bilic and K. Demeterfi, *One-dimensional QCD with finite chemical potential*, *Phys.Lett.* **B212** (1988) 83.
- [2] L. Ravagli and J. Verbaarschot, *QCD in one dimension at nonzero chemical potential*, *Phys.Rev.* **D76** (2007) 054506 [[arXiv:0704.1111](#)].
- [3] P. Rossi and U. Wolff, *Lattice QCD with fermions at strong coupling: A dimer system*, *Nucl.Phys.* **B248** (1984) 105.
- [4] F. Karsch and K.-H. Mütter, *Strong coupling QCD at finite baryon number density*, *Nucl.Phys.* **B313** (1989) 541.

- [5] S. Chandrasekharan and U.-J. Wiese, *Merlon cluster solution of a fermion sign problem*, *Phys.Rev.Lett.* **83** (1999) 3116 [[cond-mat/9902128](#)].
- [6] M. G. Alford, S. Chandrasekharan, J. Cox, and U. Wiese, *Solution of the complex action problem in the Potts model for dense QCD*, *Nucl.Phys.* **B602** (2001) 61 [[hep-lat/0101012](#)].
- [7] I. Barbour, C. Davies, and Z. Sabeur, *Lattice QCD at finite density*, *Phys.Lett.* **B215** (1988) 567.
- [8] A. Hasenfratz and D. Toussaint, *Canonical ensembles and nonzero density quantum chromodynamics*, *Nucl.Phys.* **B371** (1992) 539.
- [9] G. Aarts, O. Kaczmarek, F. Karsch, and I.-O. Stamatescu, *1/M correction to quenched QCD with nonzero baryon density*, *Nucl.Phys.Proc.Suppl.* **106** (2002) 456 [[hep-lat/0110145](#)].
- [10] B. Bringoltz, *Large-N spacetime reduction and the sign and silver-blaze problems of dense QCD*, *JHEP* **1006** (2010) 076 [[arXiv:1004.0030](#)].
- [11] J. Bloch, *Evading the sign problem in random matrix simulations*, *Phys. Rev. Lett.* **107** (2011) 132002 [[arXiv:1103.3467](#)].
- [12] J. Bloch, *A subset solution to the sign problem in random matrix simulations*, *Phys. Rev.* **D86** (2012) 074505 [[arXiv:1205.5500](#)].
- [13] J. Bloch, F. Bruckmann, M. Kieburg, K. Splittorff, and J. Verbaarschot, *Subsets of configurations and canonical partition functions*, *Phys.Rev.* **D87** (2013) 034510 [[arXiv:1211.3990](#)].
- [14] M. Lombardo, K. Splittorff, and J. Verbaarschot, *Distributions of the phase angle of the fermion determinant in QCD*, *Phys. Rev.* **D80** (2009) 054509 [[arXiv:0904.2122](#)].
- [15] G. Aarts and K. Splittorff, *Degenerate distributions in complex Langevin dynamics: one-dimensional QCD at finite chemical potential*, *JHEP* **1008** (2010) 017 [[arXiv:1006.0332](#)].
- [16] K. Langfeld and A. Wipf, *Fermi-Einstein condensation in dense QCD-like theories*, *Annals Phys.* **327** (2012) 994 [[arXiv:1109.0502](#)].
- [17] P. de Forcrand, *Simulating QCD at finite density*, *PoS LAT2009* (2009) 010 [[arXiv:1005.0539](#)].
- [18] T. D. Cohen, *Functional integrals for QCD at nonzero chemical potential and zero density*, *Phys.Rev.Lett.* **91** (2003) 222001 [[hep-ph/0307089](#)].
- [19] J. Bronzan, *Parametrization of SU(3)*, *Phys.Rev.* **D38** (1988) 1994.
- [20] P. de Forcrand, S. Kim, and T. Takahashi, *QCD simulations at small chemical potential*, *Nucl. Phys. Proc. Suppl.* **119** (2003) 541 [[hep-lat/0209126](#)].